International Journal of Nanomedicine Dovepress

Open Access Full Text Article ORIGINAL RESEARCH

Curcumin-Loaded Nanocomposite Hydrogel Dressings for Promoting Infected Wound Healing and Tissue Regeneration

Zhengzheng Fu[1,*], Jingwen Zou[1,*], Jing Zhong[1], Jipang Zhan[1], Lian Zhang[1], Xiaoru Xie[1], Lai Zhang[1,2], Wenqiang Li[3], Renliang He[1]

[1]Department of Dermatologic Surgery and Dermatologic Oncology, Dermatology Hospital of Southern Medical University, Guangzhou, Guangdong Province, 510000, People's Republic of China; [2]Guangdong Pharmaceutical University, Guangzhou, Guangdong Province, 510006, People's Republic of China; [3]Engineering Technology Research Center for Sports Assistive Devices of Guangdong, Guangzhou Sport University, Guangzhou, Guangdong Province, 510500, People's Republic of China

*These authors contributed equally to this work

Correspondence: Wenqiang Li; Renliang He, Department of Dermatologic Surgery and Dermatologic Oncology, Dermatology Hospital of Southern Medical University, Guangdong Provincial Dermatology Hospital, 2 Lujing Road, Yuexiu District, Guangzhou, Guangdong Province, 510000, People's Republic of China, Email liwq@gzsport.edu.cn; zshrl2006@smu.edu.cn

Background: The skin regulates body processes. When damaged, it is prone to breeding bacteria, causing inflammation and impeding wound healing. There is an urgent need for new dressings that can combat bacteria to aid in infectious wound repair.

Methods: In this study, a curcumin-loaded nanocomposite hydrogel dressing (GelMA/AHA-Gel@Cur) with antibacterial properties and strong toughness was synthesized, designed to combine the modified gelatin-based hydrogel (GelMA/AHA) with curcumin-coated gelatin (Gel@Cur) nanoparticles to promote the healing of bacterial infection wounds. Under UV irradiation, methylacrylylated gelatin (GelMA) and aldehyaluronic acid (AHA) formed a composite network hydrogel through radical polymerization and Schiff base reaction. Meanwhile, the residual aldehyde group on the molecular chain of AHA securely locked Gel@Cur nanoparticles in the hydrogel network through Schiff base reaction.

Results: The addition of Gel@Cur nanoparticles not only enhanced the hydrogel's mechanical strength but also facilitated a sustained, gradual release of curcumin, endowing the composite hydrogel with robust antimicrobial capabilities. In an animal model of infected wounds, the composite hydrogel significantly improved wound closure, healing, and vascularization compared to the control group. Hemocompatibility tests confirmed the hydrogel's safety, with a hemolysis ratio of just 0.45%. Histological evaluation following treatment with the composite hydrogel showed improved tissue architecture, increased collagen deposition, and regeneration of dermal gland structures.

Conclusion: The GelMA/AHA-Gel@Cur composite hydrogel exhibits excellent mechanical properties, potent antimicrobial activity, and controlled drug release, along with superior cell and hemocompatibility. These characteristics make it a promising material for infected wound repair and a potential candidate for clinical skin regeneration applications.

Keywords: Nanocomposite hydrogel dressings, infected wound repair, antibacterial properties, drug delivery

Introduction

The skin is the main protective barrier of the body against harmful invaders like bacteria and viruses, and it also plays a key part in controlling the body's metabolic functions.[1–3] However, when the skin is compromised due to factors like surgery, burns, or chronic conditions like diabetic foot ulcers, it becomes susceptible to infections.[4–6] Apart from the risk of infection, the spread of infections can lead to escalated treatment expenses, treatment inefficacy, and potentially life-threatening situations. Although traditional treatments like topical medications, gauze dressings, and autologous skin grafts offer temporary relief, they have limitations in terms of treatment duration, pain management, and scar formation. In cases of extensive or deep burns, conventional therapies often fall short in fully restoring skin function and appearance to a satisfactory level.[7–9]

Received: 31 July 2024
Accepted: 10 October 2024
Published: 18 October 2024

Graphical Abstract

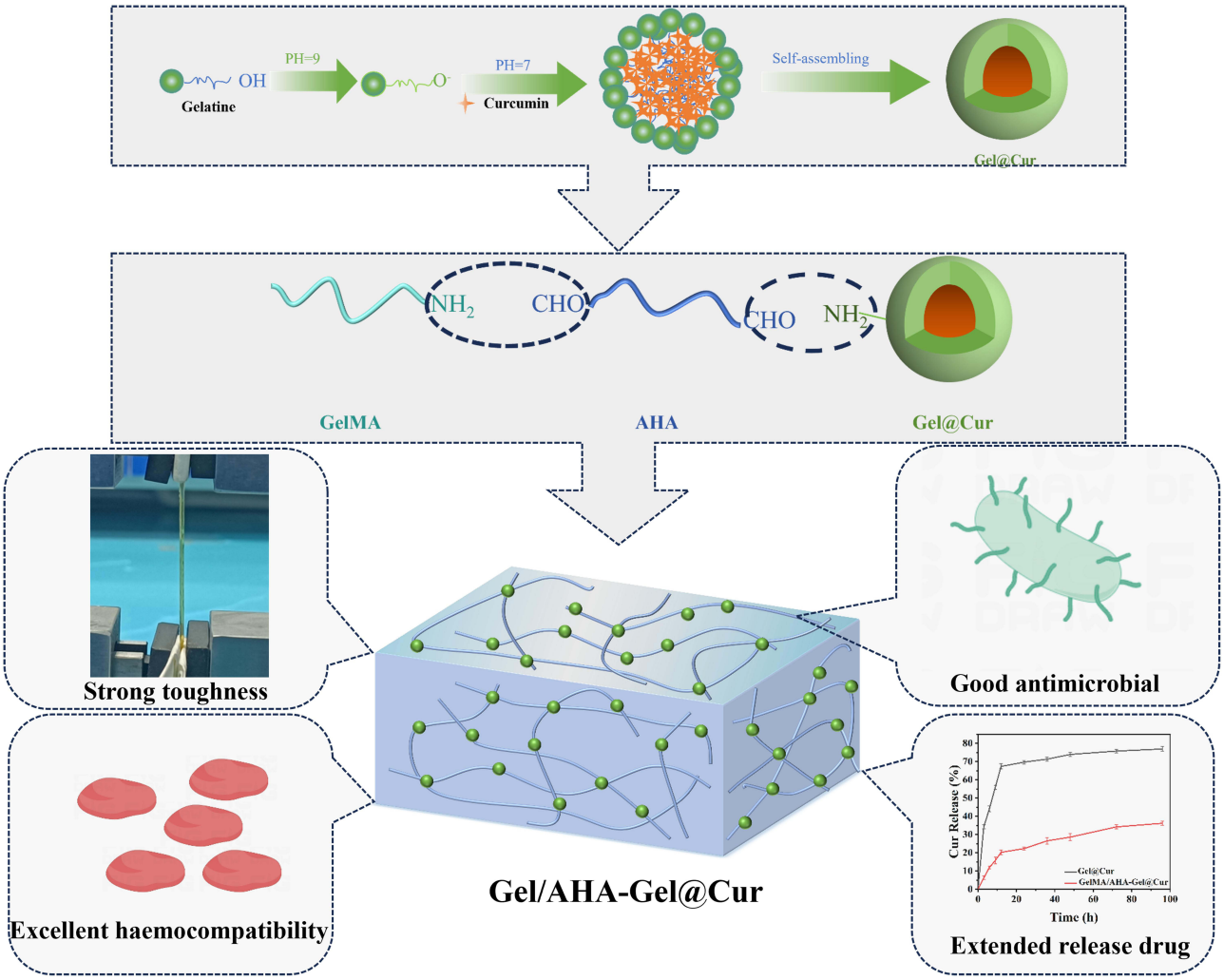

In the field of skin repair, particularly in the context of infected wounds, researchers are focused on developing novel materials with antimicrobial properties to enhance repair. Hydrogels have gained attention for their ability to mimic the extracellular matrix (ECM), creating a moist environment crucial for wound healing. They shield new cells from external harm, promote cell growth and movement, and reduce scar formation.[10–12] Gelatin (Gel) stands out among hydrogel materials for skin repair due to its biocompatibility and biodegradability. For instance, Lu[13] employed a Schiff base reaction to combine a complex formed by iron ions and 2,3,4-trihydroxybenzaldehyde with a gelatin hydrogel, thereby creating a composite hydrogel with antibacterial and anti-inflammatory properties. Xu[14] demonstrated that methacryloylated gelatin can be combined with filipin proteins to create a composite hydrogel with accelerated acute wound healing properties under UV light. Gel not only supports cell growth but also breaks down in a way that is easily metabolized by the body, minimizing long-term implantation risks.[15–17] Although gel hydrogels have advantages in promoting cell adhesion and proliferation, their antibacterial effects, especially in infected wounds, are still limited.

Topical antimicrobials have been shown to be effective in treating infected wounds. However, inappropriate use of antibiotics has also caused the development of bacterial resistance and the evolution of bacterial strains, despite the effectiveness of antibiotics in inhibiting bacteria. It is therefore important to find safer antimicrobial drugs with fewer

side effects. Curcumin (Cur) is a natural antibacterial with a superior safety profile and fewer side effects than conventional antibiotics. The structural features and antioxidant products produced by curcumin are able to inhibit bacterial growth with significant effect. However, curcumin has low water solubility and short plasma half-life,[18] and due to its rapid metabolism, which hinders its use in the repair of chronically infected wounds.

In order to solve the problem of poor water solubility and short plasma half-life of curcumin, experts and scholars have designed many pharmaceutical preparations to solve this problem. For example, Mohammed S. Alqahtani[19] used curcumin combined with lignin nanoparticles for wound tissue repair; Wu[20] used copper nanoparticles loaded with curcumin and modified the particles with hyaluronic acid to promote diabetic wound repair; The acid instability of micelles for curcumin delivery using octenylsuccinic anhydride (OSA) and cysteamine double modification has been Long used.[21] These nanoparticles can prolong the metabolism time of curcumin in the body through sustained release of curcumin, but they also bring new problems, such as lignin nanoparticles cannot be completely degraded after use; The biocompatibility of gold nanoparticles is weak, and there are risks during use. Although dextrin-based micelles have a certain degree of stability, the preparation process is complex and the preparation cost is high. Therefore, there is an urgent need for a biodegradable, biocompatible and simple preparation of nanoparticles that can be used to carry curcumin. Gelatin nanoparticles meet the above requirements, but also have good dispersibility and a large number of amino groups. After the gelatin nanoparticles were combined with the hydrogel material, the 3D structure of the hydrogel further improved the sustained drug release ability of the nanoparticles. At the same time, the nanoparticles were anchored in the hydrogel through hydrogen bonding interaction, making the drug release process more stable.

In this study, we prepared a curcumin-loaded nanocomposite hydrogel dressing (GelMA/AHA-Gel@Cur) with antimicrobial and slow-release drug properties to promote the healing of bacterially infected wounds using a modified gelatin-based hydrogel (GelMA/AHA) that combines the unique advantages of Cur and gelatin nanoparticles. The aggregation of gelatin molecular chains, driven by van der Waals and hydrophobic forces, encapsulated Cur to form Gel@Cur nanoparticles. Aldehyde-acylated hyaluronic acid (AHA) was used to immobilise the Gel@Cur nanoparticles in the network structure of the GelMA hydrogel by Schiff base reaction. Meanwhile, methacrylated gelatin (GelMA) and AHA were used to form a composite network hydrogel by radical polymerisation and Schiff base reaction (Figure 1). The resulting composite hydrogel not only showed significant antimicrobial effects, but also excellent haemocompatibility

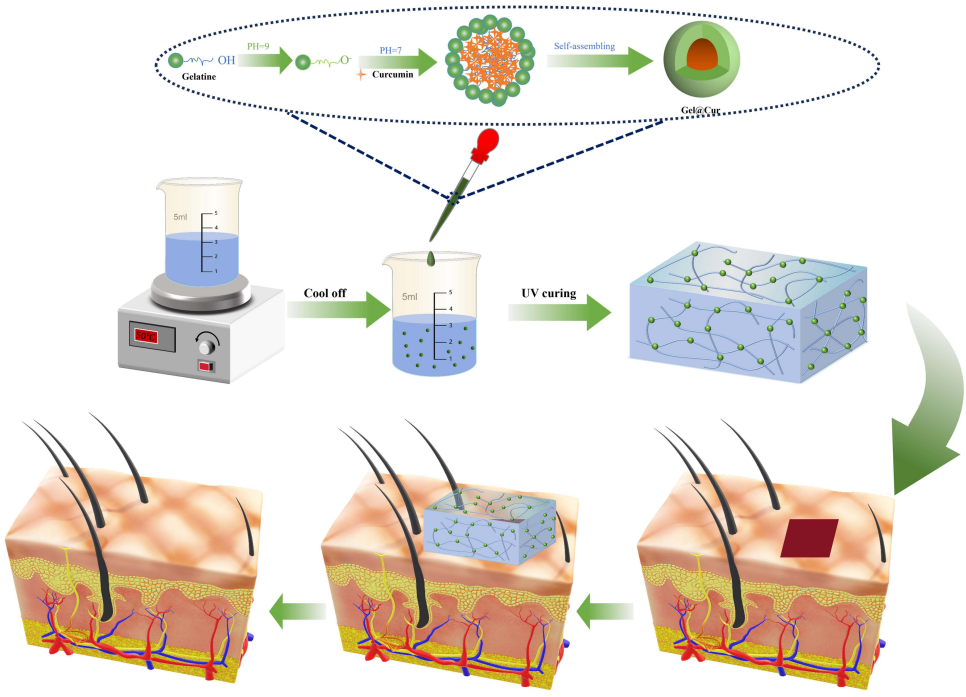

Figure 1 Preparation and application of GelMA/AHA-Gel@Cur composite hydrogels.

and biocompatibility. Furthermore, the Schiff base structure is susceptible to breakdown in the presence of acidic conditions, particularly when the wound is infected, resulting in a reduction in pH. The nanocomposite hydrogel, however, exhibits intelligent responsiveness, accelerating the release of nanomedicines in a controlled and precise manner. This approach offers a promising avenue for the treatment of infected wounds, with the potential to significantly accelerate the healing process. The properties of this hydrogel provide a valuable and innovative solution for the management of infected wounds.

Experimental and Methods

Materials

The hyaluronic acid (HA, *M*w=1.5×10^6 Da), sodium periodate (SP), and gelatin (Gel) were obtained from Shanghai Macklin Biochemical Technology Co. The curcumin (Cur) and methacrylic anhydride (MA) were provided by Aladin Reagent (Shanghai) Co. Tianjin Damao Chemical Reagent Factory provided the photoinitiator I2959. The remaining analytical grade chemical reagents were used as received, requiring no further processing.

Preparation of AHA, GelMA and Gel@Cur

AHA was originally synthesised in accordance with the literature,[22–24] by dissolving HA (*M*w = 1.5×10^6 Da, 2.0 g) in 200 mL of phosphate buffered saline (PBS) at pH 5.0. Next, the mixture was supplemented with 1.0 g of sodium periodate and placed in darkness at 25 °C for 5 h. The reaction was stopped by the addition of 2 mL of ethylene glycol, after which the combined solution was dialyzed for 5 days and then lyophilized to obtain AHA. The resulting products were characterised using Fourier transform infrared spectroscopy (FTIR) and proton nuclear magnetic resonance spectroscopy (^{1}H-NMR).

The synthesis of GelMA was conducted in accordance with a modified version of the previously reported method.[25–27] Initially, 10 g of gelatin was solubilized in 100 mL of carbonate buffer solution (pH=9) for 1 h at 25 °C. The solution was then heated to 60 °C and stirred until complete dissolution. Throughout the agitating procedure, gelatin (0.8 mL) was slowly introduced in drops, flowing at a pace of 1 mL/min, over a span of 3 h at 50 °C. The reaction was then terminated by the addition of 400 mL of deionised water at a temperature of 50 °C. Subsequently, the sample was dialysed in a 10 kD molecular weight cut-off dialysis bag for a period of one week, with four water changes per day, in order to eliminate any unreacted MA. The dialysate was 5000 rpm for 5 min, and the supernatant was frozen at −80 °C. The frozen samples were subsequently lyophilised to obtain GelMA samples, which were stored in a drying cabinet. The synthesized products were characterized using FTIR and ^{1}H-NMR.

The synthesis of Gel@Cur nanoparticles was achieved through the modification of a previously reported method, as detailed in references.[28–30] Gelatin (1.0 g) was solubilized in 100 mL of ultrapure water and heated to 45 °C with stirring for 10 min. The pH was fixed at 12.0 with 4 mol/L NaOH, after which 0.1 g of curcumin was added and the mixture was stirred continuously for 30 min. Subsequently, 1 mol/L hydrochloric acid was employed to neutralise the pH to 7.0, thereby producing Gel/Cur nanoparticles. Subsequently, the solution was subjected to centrifugation at 1375 ×g for 30 min, after which the supernatant was collected and subsequently lyophilised. The morphology of the Gel@Cur nanoparticles was examined using a scanning electron microscope (SEM, SU9000).

The synthesis steps of the GelMA/AHA-Gel@Cur hydrogel were conducted by weighing GelMA (15 wt%) and AHA (1 wt%) solids, adding an appropriate amount of deionised water, and then dissolving the mixture at 50 °C before cooling it to room temperature. Subsequently, Gel@Cur (0.1 wt%) nanoparticles and photoinitiator I29529 (0.25 wt%) were incorporated after thorough mixing. The GelMA/AHA-Gel@Cur hydrogel was then obtained through UV illumination for 5 min.

Mechanical Properties Testing of Hydrogels

The physical characteristics of the hydrogels were analyzed using a universal tensile testing apparatus (Instron, Norwood, MA, USA) with a 100 N load cell at a temperature of 25 °C. Tensile experiments were carried out on hydrogel specimens that were 40 mm long, 4 mm wide, and 7 mm tall, subjected to a tensile rate of 50 mm/min. Compression tests were

conducted on hydrogel samples with a diameter of 10 mm and a height of 20 mm to determine the maximum compressive strength required to break the samples.

Rheological Properties of Hydrogels

The characterization of the rheological properties was carried out using a rheometer (DHR-1, TA Instruments, New Castle, DE, USA) equipped with a UV cross-linking device. Time scans were first performed at a constant strain rate of 1.0% and a corner frequency of 10.0 rad/s on the viscous hydrogel precursor under 10 mW/m^2 UV irradiation. Frequency scan tests at a fixed strain of 0.5% and a cut-off frequency of 10.0 rad/s were then performed in the linear viscoelastic region of the hydrogel system. Finally, at a fixed angular frequency of 10.0 rad/s, strain amplitude scanning tests were performed. A temperature of 37°C was used for all tests.

In vitro Antimicrobial Evaluation

The antibacterial properties of the materials were assessed by exposing hydrogels to Escherichia coli (*E. coli*, BeNa Culture Collection, China) and Staphylococcus aureus (*S. aureus*, BeNa Culture Collection, China).[31–33] The hydrogels were immersed in PBS and then placed it in Luria-Bertani (LB) medium with bacterial suspensions at a concentration of 10^6 CFU/mL. Each sample was incubated on a shaker at 37 °C for varying durations of 2, 4, 6, 8, 21, and 30 h. After incubation, the bacterial suspensions were collected and analyzed using turbidimetric analysis with an enzyme marker (Biotek Synergy H1) at 620 nm. The experiment was conducted with three parallel replicates.

Swelling and Drug Release Tests

In the present study, the swelling behavior of the hydrogel was investigated by gravimetric analysis. The initial weight (W_d) of the hydrogel was determined, and then it was immersed in PBS. The hydrogel was removed and replaced with new PBS every 12 h, and the gel weight was measured using an electronic balance (Li Chen, Ningbo Huifeng Instrument Factory, China), and the W_s is denoted as the sample mass at different time periods. The specific swelling ratio was then determined using Eq. (1).[34–36]

$$\text{Swelling ratio}(\%) = \frac{W_s}{W_d} \times 100\% \tag{1}$$

To study the in vitro drug release behavior of nanoparticles and composite hydrogels, the nanoparticles and the composite hydrogel based on equal mass nanoparticles were immersed in PBS (0.1 M) at an extraction ratio of 0.8 mg/mL, placed at 37 °C, and the nanoparticles were extracted at a concentration of 0.8 mg/mL. 4 mL of the extract was taken at 3, 6, 9, 12, 24, 48, 72, and 96 h, and the absorbance of the extract at 424 nm was measured with a UV spectrophotometer (L5S, INESA Shanghai Instrument and Equipment, China).

To further explain the release mechanism of Cur within the composite hydrogel, we performed a kinetic evaluation of the in vitro release data. The composite hydrogel drug release data were fitted to four common kinetic models, namely zero order (Eq. (2)), first order (Eq. (3)), Korsmeyer-Peppas (Eq. (4)) and Higuchi (Eq. (5)) models:[37,38]

$$Q = k_0 t \tag{2}$$

$$\text{Ln}Q = \text{Ln}Q_0 - k_1 t \tag{3}$$

$$\text{Ln}Q = n\text{Ln}t + \text{Ln}k_p \tag{4}$$

$$Q = k_H t^{\frac{1}{2}} \tag{5}$$

where Q, k_0, k_1, n and k_H are the cumulative Cur release percentages and the Cur release rate constants for the zero order, first order, Korsmeyer-Peppas and Higuchi models respectively.

In vitro Cell Testing

Cytocompatibility Evaluation

The cytocompatibility of the material was evaluated by exposing human umbilical vein endothelial cells (HUVECs, Provided by Wuhan Shane Biological Co., LTD., China) to hydrogel extracts. Hydrogel cylinders with a diameter of 7 mm and a thickness of 1 mm were prepared, freeze-dried, exposed to UV irradiation for 24 h, and then immersed in DMEM medium for an additional 24 h. HUVECs were in vitro cultured at a density of 1.5×10^4 cells/well in 48-well plates (Gibco) containing DMEM medium. The cells were cultivated under 5% CO_2 at 37 °C for 5 days, with three replicates per hydrogel sample. Cytotoxicity was evaluated by quantifying the absorbance at 450 nm using a CCK-8 (Wuhan Optics Valley Biomedical Co., China). The viability of the cells was assessed by staining them with acridine orange/ethidium bromide (AO/EB) and observing them under an inverted fluorescence microscope.[39–41]

Scratch Evaluation

The experiment began with cells being seeded in 6-well culture plates, each well containing a density of 5×10^5 cells. Once the cells had formed a monolayer, meticulous scraping was performed using pipette tips to create a uniform scratch on the cell surface. Subsequently, the cells were carefully washed with PBS to remove any cellular debris resulting from the scraping process. Following the washing step, the cells were exposed to a culture medium, specifically DMEM, which contained the material extract under investigation. The progression of scratch closure was closely monitored using an inverted microscope, with observations recorded at the initial time point (0 h) and after 24 h. To quantify the extent of scratch closure, image analysis software was employed to measure the area of the scratch at both time intervals. The ratio of cell migration, indicating the ability of the cells to move and cover the scratched area, was calculated using a specific Eq. (6).[34–36]

$$\text{Migration Rate}(\%) = \frac{R_0 - R_t}{R_0} \times 100\% \tag{6}$$

where R_0 represents the initial scratch area and R_t represents the remaining scratch area at time t.

Cell Proliferation and Adhesion

HUVECs were plated in 96-well plates at a concentration of 1×10^5 cells/mL and cultured in DEME medium at 37 °C for 5 days. After incubation, the cells were rinsed with PBS and fixed with 4% paraformaldehyde. Following fixation, the cells were permeabilized with 0.1% Triton X-100 and blocked with 1% BSA. Subsequently, staining for the cytoskeleton was performed using rhodamine-labelled ghost pen cyclopeptide, while the nucleus was stained with DAPI solution, both under light-avoidance conditions. Visualization of cell proliferation and adhesion status was conducted using laser scanning confocal microscopy with excitation/emission wavelengths set at 405/552 nm.[39–41]

Angiogenesis

Initially, 10 μL of matrix gel was uniformly distributed across all wells of a 96-well plate and left to incubate at 37 °C for 30 min to create a gel layer. Subsequently, human umbilical vein endothelial cells (HUVECs, 5000 cells/well) were seeded onto the gel layer and allowed to adhere for 2 h. Following a 6-hour incubation period, the HUVECs started to develop tubular structures, indicating the initiation of the angiogenic process.

Haemocompatibility and Wound Healing Tests

Haemocompatibility

Samples were immersed in 2 mL of a 2.5% wt/vol plasma suspension from SD rats (Guangdong Experimental Animal Centre), which had been diluted with saline solution (medicine), and 1 h was allowed for incubation at 37 °C with a shaking speed of 120 rpm. Positive and negative controls were prepared by diluting plasma (2.5% by weight) with 2 mL of water and Saline solution (medicine), respectively. After the erythrocyte solution had been incubated, it was collected and subjected to centrifugation at 3000 rpm for 5 min. Subsequently, 100 μL of the supernatant was deposited into a 96-well plate and the absorbance was recorded at 540 nm. These values were recorded as A_S, A_N, and A_P, respectively. The haemolysis rate was then calculated using Eq. (7):[42]

$$\text{Hemolysisrate}(\%) = \frac{A_S - A_N}{A_P - A_N} \times 100\% \quad (7)$$

where A_S represents the absorbance value of the sample supernatant, and A_P and A_N are the absorbance values of the supernatant of the positive and negative control groups, respectively.

In vivo Infected Wound Repair Evaluation

All animal treatments were authorized by the Experimental Animal Ethics Committee of Guangdong Pharmaceutical University (serial number: gdpulacspf2022431) and conducted in accordance with the university's Guidelines for Care and Use of Laboratory Animals. This research involved the use of 12 SD rats (250–300 g) procured from the Guangdong Experimental Animal Centre to explore the healing properties of hydrogels. Sodium pentobarbital (25 mg/kg) was used to induce unconsciousness in the rats, after which three circular wounds of 7 mm in diameter were carefully made on their dorsal area using a 7 mm puncture device. A sterilized cotton swab soaked in Staphylococcus aureus solution (10^6 CFU/mL) was applied to the wounds on the mice. One wound remained untreated as a control, while the other two wounds received treatment with nanoparticles and hydrogel dressings. The hydrogel was administered to the wounds and secured in place using Vaseline gauze and an elastic bandage. The application of the hydrogel was fixed onto the wound location with Vaseline gauze and an elastic bandage. The progress of wound closure was observed and documented using a digital camera on days 0, 3, 5, 7, 9, and 14, and the rate of wound healing was calculated. Six rats were randomly euthanized on days 7 and 14 post-wound recovery. Tissue specimens from the wound site and neighboring regions were obtained, preserved in 10% paraformaldehyde solution, enclosed in paraffin, and then evaluated using Hematoxylin and Eosin (H&E) and Masson staining to evaluate tissue structure, regeneration, and collagen accumulation.[43–45]

Immunohistochemistry

To better understand the process of neovascularization during wound healing, this study employed immunohistochemistry methods to detect specific markers in tissue sections on the seventh day. The tissue samples were incubated with primary antibodies targeting CD31 or α-SMA at 4 °C overnight. Fluorescently labeled secondary antibodies were used for detection: rhodamine-labeled goat anti-rabbit for CD31 and FITC-labeled goat anti-mouse for α-SMA. The nuclei were counterstained with DAPI to facilitate observation. Confocal laser scanning microscopy (CLSM, Leica TCS SP8, Leica Microsystems, Germany) was utilized to analyze immunofluorescence-labeled sections and assess the expression of CD31 and α-SMA. Quantitative fluorescence image analysis obtained via CLSM was conducted using Image J software, providing data on CD31 and α-SMA expression.

Statistical Analysis

The statistical analysis involved utilizing means and conducting various statistical tests, including paired t-tests and one-way ANOVA, on data that had been normalized using SPSS software. Significance levels were indicated as: * for $p \leq 0.05$, ** for $p \leq 0.01$, and *** for $p \leq 0.001$.

Results and Discussion

Characterization and Analysis of AHA, GelMA and Gel@Cur

As the gelatin solution transitions from alkaline to neutral, the reduction in charge repulsion between gelatin molecules allows intermolecular hydrogen bonding and van der Waals forces to become predominant, facilitating interactions between gelatin molecules and the formation of nanoparticles. The scanning electron microscope (SEM) images of these nanoparticles are depicted in Figure 2a. The particle size distribution was analyzed using ImageJ, and the statistical findings are presented in Figure 2b. The comprehensive map and particle size distribution plot demonstrate that the gelatin nanoparticles prepared exhibit a relatively uniform size distribution, with an average particle diameter of 0.181 μm.

AHA was synthesized through an oxidation reaction between HA and $NaIO_4$, and its synthesis was confirmed using FTIR and ^{1}H-NMR analysis (Figure 2c and d). The emergence of new peaks at 1731 cm^{-1} and δ= 5.0, 5.11, and 5.19 ppm in the AHA sample indicated the presence of aldehyde groups in the HA structure. This observation aligns with

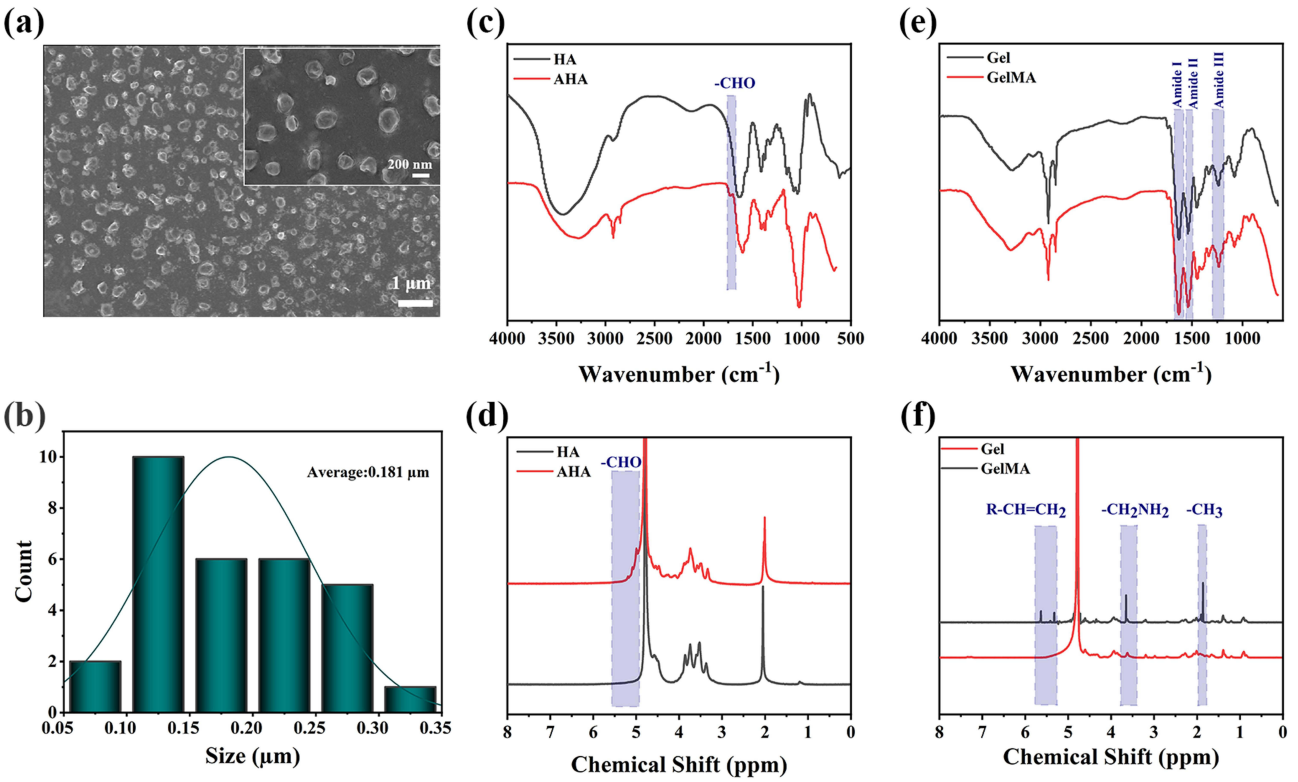

Figure 2 (**a**) SEM pattern of Gel@Cur nanoparticles. (**b**) Particle size distribution of Gel@Cur nanoparticles. (**c**) FTIR pattern of AHA and (**d**) ^{1}H-NMR pattern of AHA. (**e**) FTIR pattern of GelMA and (**f**) ^{1}H-NMR pattern of GelMA.

existing literature and confirms the successful preparation of AHA samples with aldehyde groups.[46] Similarly, GelMA, as shown in Figure 2e and f, still exhibited characteristic bands of the gel backbone, such as amide (I), amide (II), and amide (III), in comparison to gel. The peaks at δ= 1.86, 3.66, 5.32, and 5.64 ppm were attributed to the introduction of a new functional groups in the gel, consistent with literature reports,[47] signifying the successful preparation of GelMA samples.

Mechanical and Rheological Analysis of Hydrogels

In accordance with the experimental protocol, GelMA, GelMA/AHA and GelMA/AHA-Gel@Cur hydrogel samples were prepared and subjected to mechanical testing in compression and tension. Concurrently, the rheological properties of the three groups of hydrogels with identical dimensions were evaluated, and the results of the tests are presented in Figure 3. The results of the compressive mechanical tests were presented in Figure 3a–c, indicating that the three groups of hydrogels exhibit similar compressive stress-strain curves. However, Figure 3d–f showed that the hydrogel group with the addition of Gel@Cur nanoparticles displayed superior tensile properties. To gain a clearer understanding of how the nanoparticles affect the hydrogel's mechanical behavior, we calculated the compressive and tensile elastic moduli for each group of hydrogels, as illustrated in Figure S1. The addition of Gel@Cur nanoparticles resulted in a decrease in both the compressive and tensile elastic moduli of the composite hydrogel. This decrease is due to the steric hindrance effect of the Gel@Cur nanoparticles, which disrupts the chemical cross-linking within the hydrogel, leading to a reduction in the cross-linking density. As depicted in Figure 3g, the storage modulus (G′) consistently exceeded the loss modulus (G″) for the hydrogels in each group, signifying that the hydrogels predominantly displayed elastic behavior across the tested frequency range. The stability of the dynamic modulus for the hydrogels in each group over a broad frequency spectrum indicates that the cross-linked system of the hydrogels established a stable network structure. The time scanning experiment, presented in Figure 3h, demonstrated that the incorporation of AHA and Gel@Cur did not influence the gelation time of the system, with the hydrogels in each group reaching gelation in approximately 150 s. Figure 3i presents the strain scan test outcomes for the hydrogels. It is evident that the storage modulus of the GelMA/AHA hydrogel

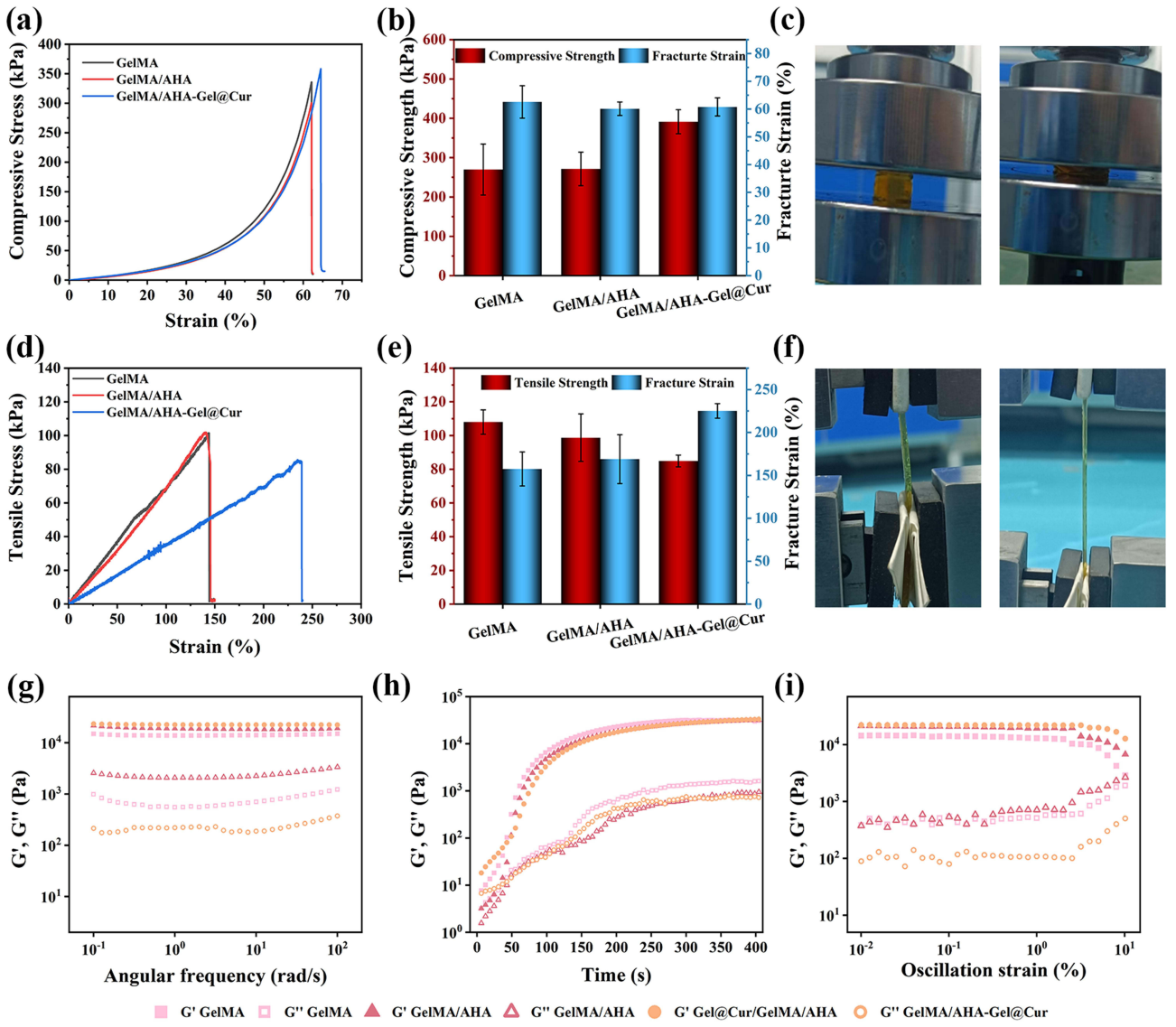

Figure 3 (**a**). Compressive stress-strain curves of hydrogels. (**b**). Compressive strength and strain at break of hydrogels. (**c**). Compression test images of hydrogels. (**d**). Tensile stress-strain curves of hydrogels. (**e**). Tensile strength and elongation at break of hydrogels. (**f**). Tensile test images of hydrogels. (**g**). Frequency scanning rheological test of the hydrogels. (**h**). Time scanning rheological test of hydrogels. (**i**). Strain scan rheological test on hydrogels.

surpasses that of the GelMA hydrogel alone. This enhancement is attributed to the formation of an additional chemical cross-linking structure through a Schiff base reaction within the GelMA/AHA hydrogel, which effectively boosts the storage modulus (G′) of the system. Furthermore, the storage modulus (G′) of the GelMA/AHA-Gel@Cur hydrogel is higher than that of the GelMA/AHA hydrogel. This increase can be ascribed to Gel@Cur nanoparticles can form non-covalent interactions, such as hydrogen bonds, with the hydrogel network.[18] These hydrogen bonds contribute to an elevated storage modulus (G′) due to their energy dissipation effect.

In vitro Antimicrobial Evaluation

It is crucial to acknowledge the significance of in vitro antimicrobial activity for materials utilized in skin repair. The antibacterial properties of various hydrogels were evaluated in this study using *S. aureus* and *E. coli*. The results are presented in Figure 4a, GelMA hydrogel and GelMA/AHA hydrogel showed higher bacterial survival compared to the control. The elevated bacterial survival ratio and reduced antibacterial activity observed with GelMA and GelMA/AHA, as compared to the control, can be attributed to the fact that both GelMA and AHA are derived from modifications of

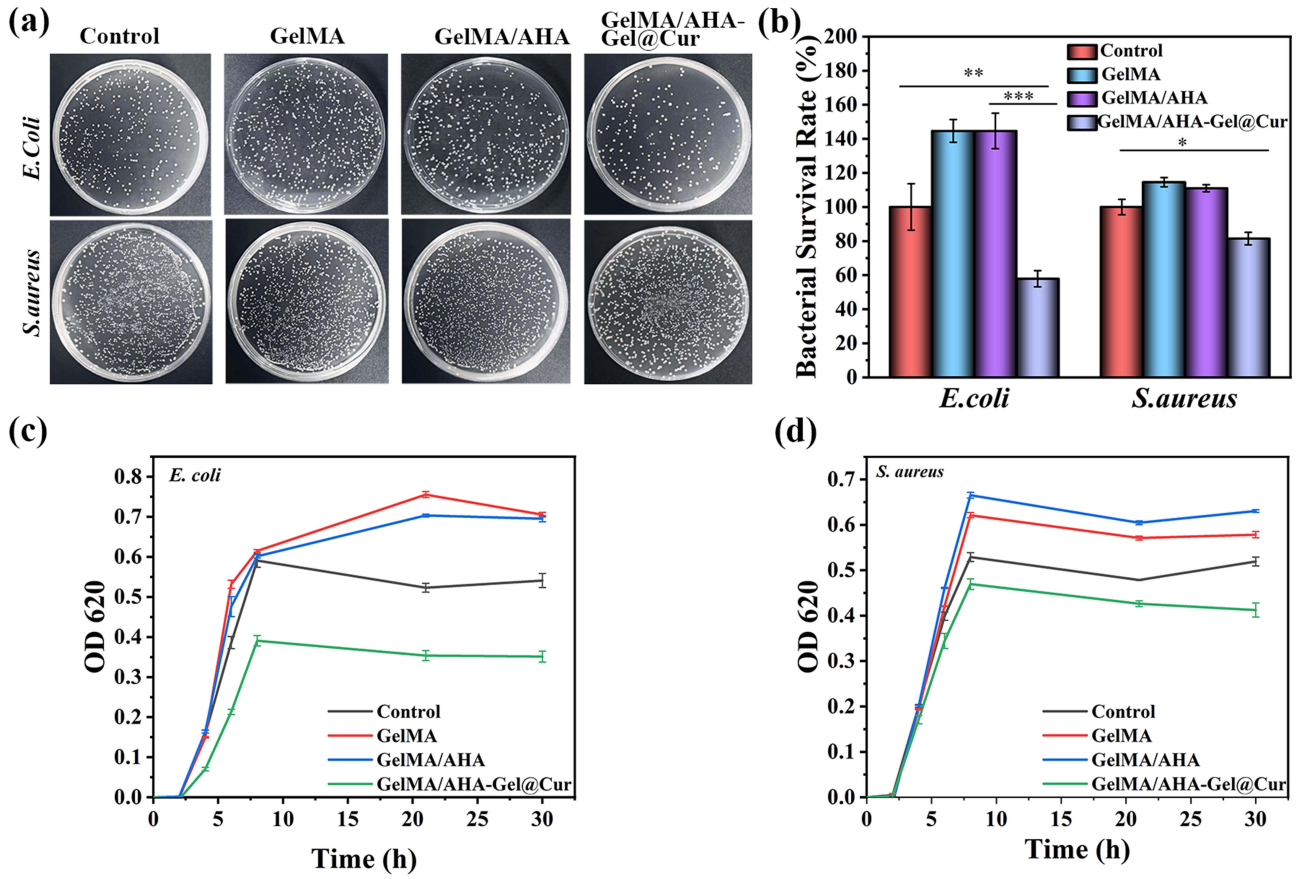

Figure 4 (**a**). Images of *E. coli* and *S. aureus* colonies after 6 h of co-culture with hydrogels. (**b**). Relative bacterial survival of *S. aureus* and *E. coli* after 6 h of co-culture with hydrogels. (**c**). Growth curve of *E. coli* co-cultured with hydrogels. (**d**). Growth curves of *S. aureus* co-cultured with hydrogels. * for $p \leq 0.05$, ** for $p \leq 0.01$, and *** for $p \leq 0.001$.

gelatin and hyaluronic acid, respectively. Gelatin and hyaluronic acid, which are important components of the extracellular matrix, do not possess antibacterial properties but are biocompatible, and the incubation of bacteria with them provides additional nutrients for bacterial growth and reproduction. Therefore, the survival rate of bacteria in the GelMA and GelMA/AHA groups was higher than that in the control group, while the antibacterial effect was lower than that in the control group. Nevertheless, the number of bacterial colonies within the GelMA/AHA-Gel@Cur hydrogel was found to be lower than that of the control group, likely due to the presence of nanoparticles containing curcumin. This trend was also reflected in the quantitative analysis illustrated in Figure 4b, demonstrating that GelMA/AHA-Gel@Cur hydrogel displayed significant antibacterial efficacy. This effect was primarily attributed to the curcumin-loaded nanoparticles, which possess remarkable antimicrobial properties. Figure 4c and d show the bacterial growth curves obtained by incubating the three hydrogel extracts with two bacteria for 30 h. The data in the figure show that the bacterial density of the GelMA/AHA-Gel@Cur hydrogel was lower than that of the control group after 30 h. This phenomenon is due to the fact that structurally, the drug loaded with nanoparticles of GelMA/AHA-Gel@Cur was riveted inside the hydrogel, which makes the hydrogel have the ability of slow release of drugs, which is reflected in the performance of the hydrogel. GelMA/AHA-Gel@Cur hydrogel has in vitro antibacterial effect.

Swelling of Hydrogels and Drug Release in vitro

The gravimetric analysis was employed to examine the swelling behaviour of the hydrogels. Figure 5a demonstrates that the swelling rate of the GelMA/AHA-Gel@Cur hydrogel reached 150%, indicating its exceptional capacity for water absorption and storage. It was observed that the swelling ratio of the GelMA/AHA-Gel@Cur hydrogel is greater than that of the GelMA and GelMA/AHA hydrogels. This suggests that the presence of curcumin-containing nanoparticles led to

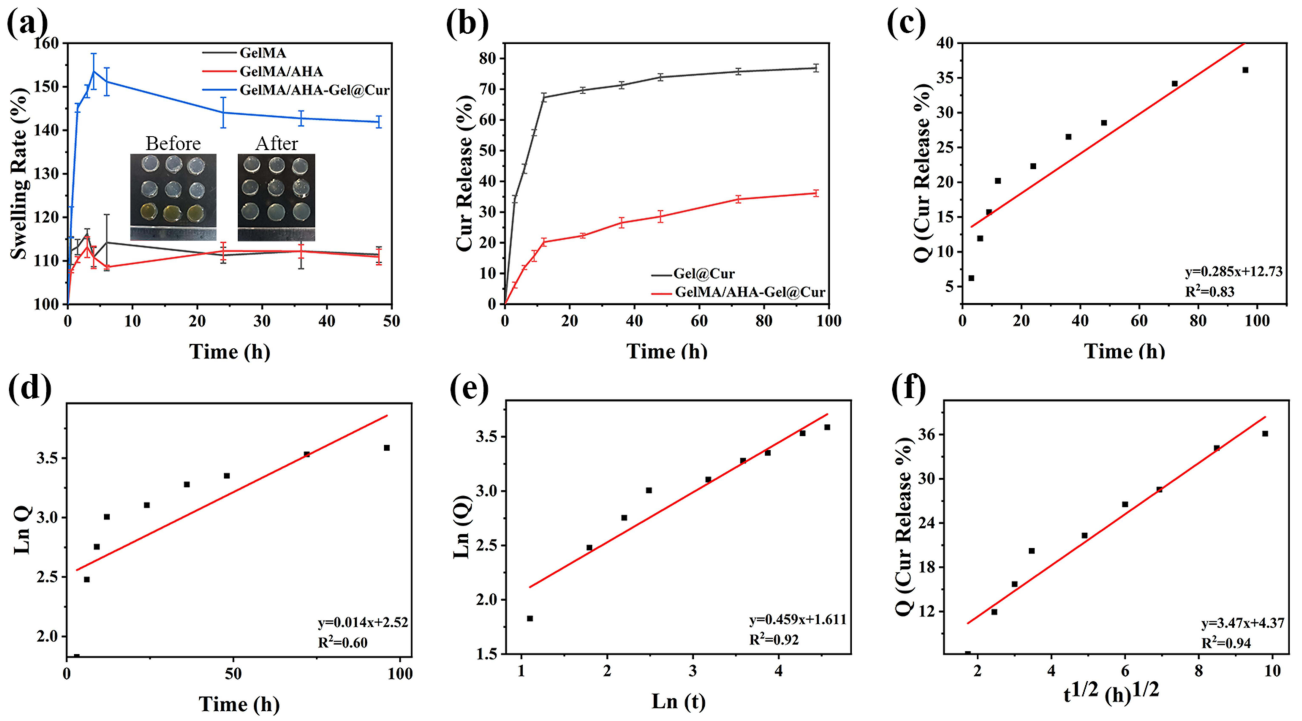

Figure 5 (**a**). Swelling rate of each group of hydrogels. (**b**). Curcumin release profile of hydrogels and nanoparticles in vitro over 96 h. (**c**). In vitro release of composite hydrogels. Zero level release simulation, (**d**). First step release simulation, (**e**). Korsmeyer-Peppas model simulation. (**f**). Higuchi model simulation.

an enhanced pore structure in the hydrogel. This observation aligns with the structural characteristics revealed by the material's mechanical properties.

To understand the release of curcumin from the hydrogel, the body fluid environment was simulated with PBS at 37°C and the absorbance of the liquid was tested at 424 nm using a UV spectrophotometer (L5S, INESA Shanghai Instrument and Equipment, China). Figure 5b shows the test results. The nanoparticles encapsulated in the hydrogel can release curcumin for more than 96 h. This ability to maintain drug concentration in the wound for an extended period of time is beneficial to the repair and treatment of infectious wounds. To further investigate the drug release mechanism of GelMA/AHA-Gel@Cur hydrogel, four commonly used drug release models were used to fit the drug release of GelMA/AHA-Gel@Cur hydrogel. Figure 5c–f shows that the release pattern of the drug in the hydrogel is more consistent with the Higuchi model (R^2 = 0.94), indicating that the drug release is mainly controlled by the diffusion of the drug in the medium, which belongs to non-Fick diffusion.

To gain more insight into the drug release mechanism of the composite gel, the drug release time was extended to 240h. Four drug release models were used to fit the release process. As shown in Figure S2 a–e. It can be seen from the data in the figure that there was drug burst release behavior in the hydrogel attachment at 120 h, and the model fitting results showed that the drug release behavior of the hydrogel was more consistent with the Korsmeyer-Peppas model (R^2=0.9809). Notably, with a model coefficient n value of 0.5855 (greater than 0.45), the drug release mechanism is identified as non-Fick diffusion and skeleton lysis mechanisms operate concomitantly.[48]

In vitro Analysis of Cell Viability, Migration and Tube Formation

Ensuring that wound healing materials possess excellent cytocompatibility is crucial. In order to assess the cytocompatibility of the composite hydrogel, human umbilical vein endothelial cells (HUVEC) were cultured using DEME-impregnated hydrogel with prepared medium. Cell viability was assessed on days 1, 3 and 5 using the CCK-8 kit. As illustrated in Figure 6a and b, cells cultured with GelMA/AHA-Gel@Cur infusion showed significantly higher proliferative activity over time compared to both the control group and Gel@Cur. This increased activity is attributed to the introduction of GelMA, which is derived from gelatin modification, and AHA, a derivative of hyaluronic acid. Gelatin

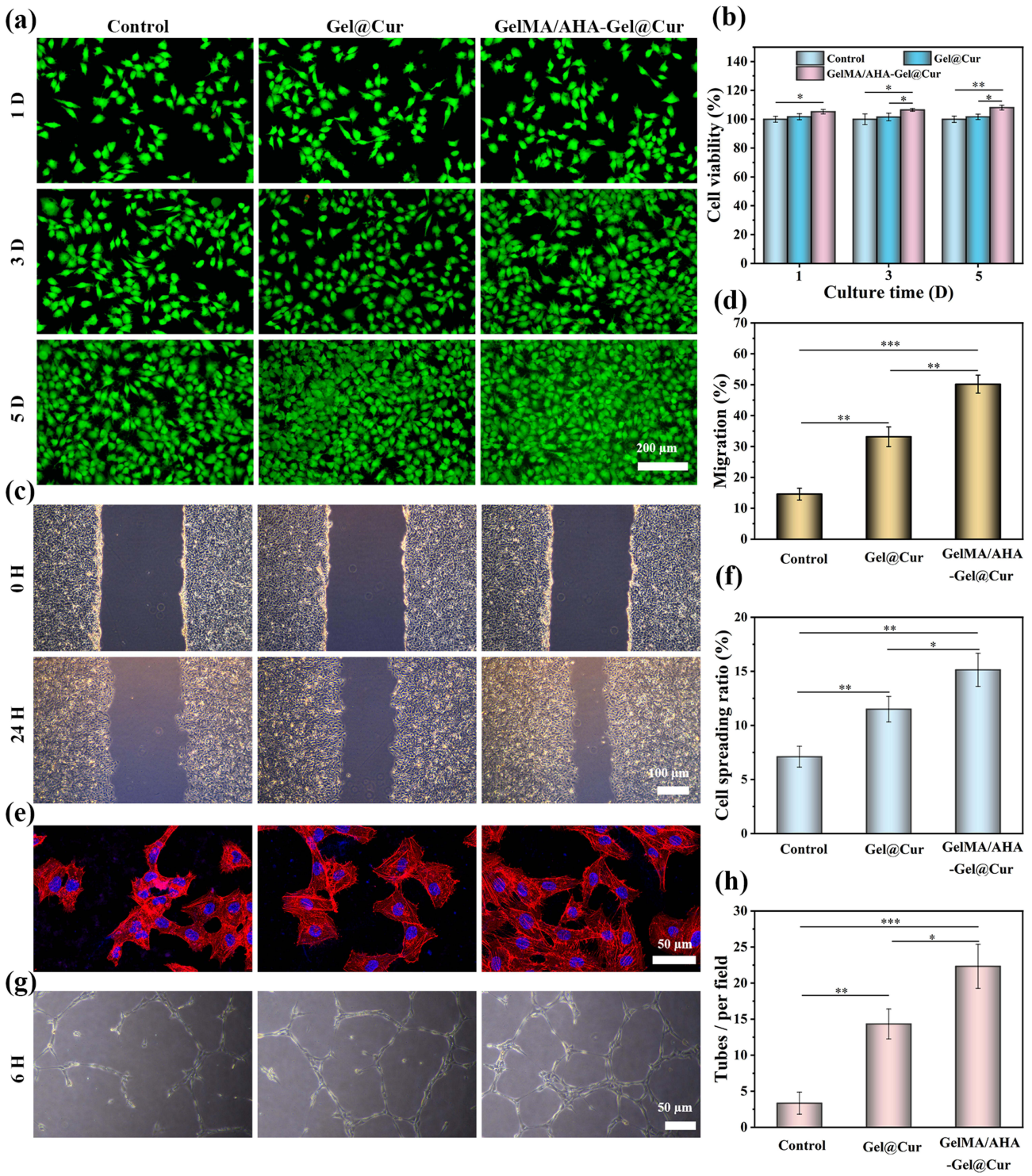

Figure 6 (**a**) Live/dead staining image assay of cells cultured with hydrogel extracts for 1, 3 and 5 days. (**b**) Quantitative assay of cell viability. (**c**) Micrographs of HUVECs migration. (**d**) Quantitative assay of HUVECs migration. (**e**) Laser confocal photographs of HUVECs cytoskeleton. (**f**) Statistical results of HUVECs spreading ratio. (**g**) HUVECs tube formation images. (**h**) Statistical results of HUVECs tube formation. * for $p \leq 0.05$, ** for $p \leq 0.01$, and *** for $p \leq 0.001$.

and hyaluronic acid are important components of the extracellular matrix and have excellent biocompatibility, promoting cell growth and reproduction. Consequently, human umbilical vein endothelial cells (HUVECs) demonstrated strong adhesion and progressively formed cell colonies.

The hydrogels' ability to support cell migration was assessed by observing the movement of HUVECs in vitro, as depicted in Figure 6c and d. The findings from the experiment showed that, in relation to cell migration, the cells grown in the GelMA/AHA-Gel@Cur hydrogel blend displayed a notably quicker migration pace, achieving a migration ratio of 50.31% of cells within 24 h, significantly surpassing the rates of the other test groups. This phenomenon is partly due to the presence of more gelatin molecules in the composite gels, and the cells are able to recognize the unique RGD (Arg-Gly-Aspartic acid) sequence of gelatin molecules for signaling, adhesion and proliferation.[49] On the other hand, the slow release of curcumin can reduce the oxygen stress effect among cells to promote better cell growth.[18] To gain further insight into the impact of material groups on the spreading of HUVECs cells, actin and cell nuclei were stained using ghost pen cyclic peptide (red) and DAPI (blue) solutions, respectively. The results obtained are presented in Figure 6e and f. The images demonstrate that GelMA/AHA-Gel@Cur exhibits a greater abundance of filamentous actin, indicating that the incorporation of GelMA and AHA into the nanoparticles enhances their cytocompatibility.

The effect of the hydrogel on HUVEC angiogenesis was analysed using the images and data shown in Figure 6g and h. The results demonstrated that after 6 h of incubation, the GelMA/AHA-Gel@Cur group exhibited the greatest blood vessel length and the highest tube number, which were significantly different from those observed in the other groups. This indicated that the hydrogel had more prominent effects on promoting angiogenesis. This phenomenon is achieved by the introduction of GelMA and AHA, which improve the biocompatibility of the nanoparticles. Furthermore, the nanoparticle-loaded hydrogel possessed the ability to continuously slow release of curcumin, which helped to create an anti-inflammatory environment, improve cell survival, and protect the cells from oxidative stress through the antioxidant properties of curcumin, damaged the extracellular matrix, thus accelerating the skin's repair process.

Evaluation of Haemocompatibility and Wound Healing

The hemocompatibility of a local wound dressing is crucial for its safety and effectiveness. Figure 7a demonstrates that Gel@Cur nanoparticles had a high level of hemocompatibility. When GelMA and AHA are added, the resulting GelMA/AHA-Gel@Cur hydrogel shows a hemolysis ratio of only 0.45%, well below the accepted safety threshold of 5%. This indicates excellent hemocompatibility of the GelMA/AHA-Gel@Cur hydrogel. The inclusion of GelMA and AHA improves the hydrogel's hydrophilicity, reducing red blood cell adhesion and minimizing cell damage.

To further investigate the impact of hydrogel on infected skin wound repair, the wound healing efficacy of hydrogel was assessed using a rat back skin wound infection model. Results depicted in Figure 7b demonstrate that both the Gel@Cur and GelMA/AHA-Gel@Cur groups exhibited accelerated wound healing rates compared to the blank control group. This enhancement was noticeable from the third day and became more prominent by the fourteenth day, owing to the antimicrobial properties of curcumin that aid in wound healing. Quantitative analysis presented in Figure 7c highlights distinctions between the Gel@Cur and GelMA/AHA-Gel@Cur groups, attributed to the hydrogel's capacity to efficiently seal wounds, foster cell proliferation, gradually release curcumin, and resist bacterial infiltration.

In order to gain further insight into the healing of the skin wound, histological examination was conducted. The H&E staining of tissue sections in Figure 7d revealed that at day fourteen of wound healing, there was a marked reduction in the number of blood vessels and the extent of epithelialisation in the Gel@Cur group compared to the composite hydrogel group. Furthermore, there was a lack of substantial regeneration of mature dermal glandular cavities and persistent inflammation at the wound site in the Gel@Cur group. Conversely, the periwound tissue in the GelMA/AHA-Gel@Cur hydrogel group displayed aligned morphology and exhibited notable regeneration of dermal glandular cavities. The incorporation of nanoparticles in the hydrogel, on the one hand, increases the time and concentration of the drug staying on the infected wound, and on the other hand, the unique 3D structure of the gel material itself, which can effectively block bacteria, maintain the moist environment of the affected area, and promote the repair of infected wounds. The duration and concentration of the drug applied to the infected wound also influenced the observed outcomes., which was reflected in the Masson-stained images (Figure 7e). These images exhibited an increase in collagen accumulation in all groups, with relatively sparse collagen accumulation in the control group and tightly aligned and organised collagen accumulation in the Gel@Cur and GelMA/AHA-Gel@Cur groups. Notably, the GelMA/

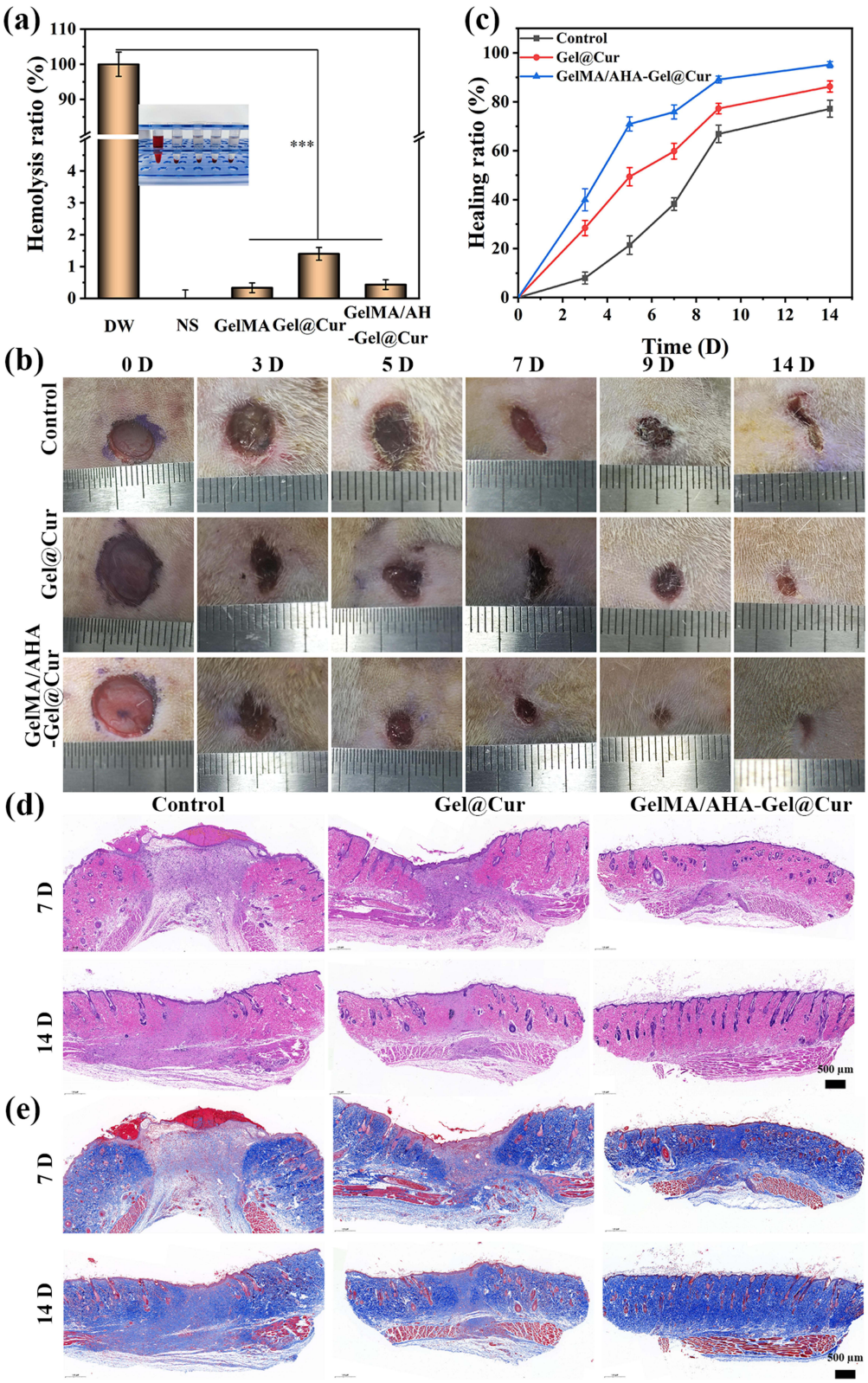

Figure 7 (**a**). Evaluation of the haemocompatibility of hydrogels. (**b**) Images of wound sites in mice after 0, 3, 5, 7, 9 and 14 days under different treatment conditions. (**c**) Wound healing ratio in mice. (**d**) Images of H&E staining and (**e**) Masson staining of skin tissue at the wound site of mice after 7 and 14 days of different treatments. Scale bar: 500 μm. *** for $p \leq 0.001$.

AHA-Gel@Cur composite hydrogel appeared to have significantly regenerated mature dermal glandular lumens compared to the Gel@Cur group. Collectively, these findings suggest that the GelMA/AHA-Gel@Cur composite hydrogel possesses the ability to promote infected wound healing.

Immunohistochemistry

Immunohistochemical manipulations were conducted on the seventh day of treatment to analyze the infected wound tissues. α-SMA was utilized to identify myofibroblasts in the wound tissues, while CD31 was used to identify endothelial cells. Figure 8a displays the experimental results, showing that the GelMA/AHA-Gel@Cur group exhibited stronger fluorescence signals for α-SMA and CD31 compared to the blank group and the Gel@Cur group. This suggests that the hydrogel group had a superior ability to repair infected wounds. The hydrogel group showed enhanced infected wound healing capabilities, with increased presence of myofibroblasts and endothelial cells on the seventh day of treatment. The quantitative analysis of the experimental data was performed using ImageJ, and the results are presented in Figure 8b and c. The repaired wound

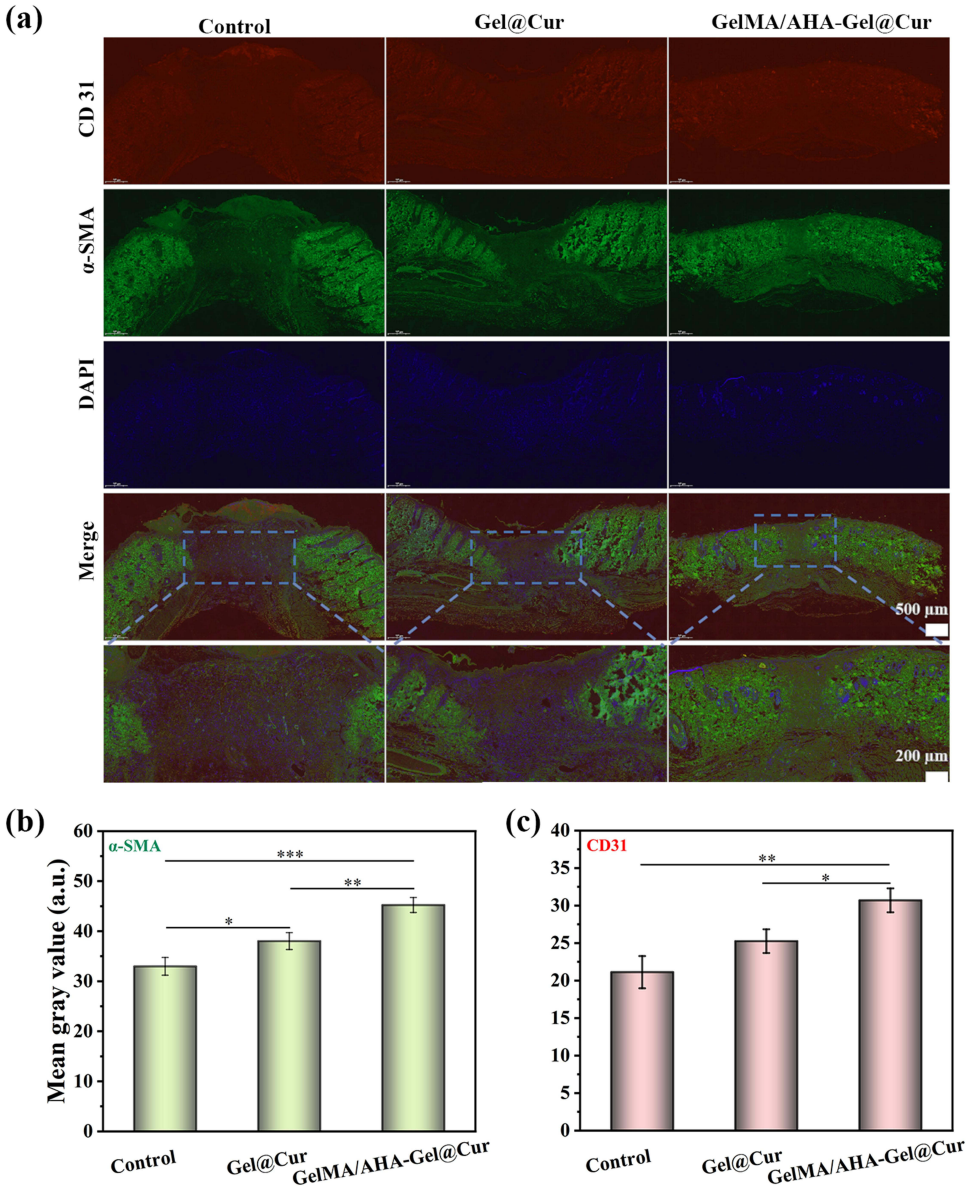

Figure 8 (**a**) Immunofluorescence staining images of infected wound tissue after 7 days treatment with different infected wound repair materials. CD31 (red), α-SMA (green) and DAPI (blue). (**b**). Relative fluorescence intensity of CD31 protein. (**c**) Relative fluorescence intensity of α-SMA protein. * for $p \leq 0.05$, ** for $p \leq 0.01$, and *** for $p \leq 0.001$.

tissues in the hydrogel group had a significantly higher number of myofibroblasts and endothelial cells on the seventh day compared to other groups. Overall, these results support the conclusion that the GelMA/AHA-Gel@Cur composite hydrogel is highly effective in repairing infected wounds, suggesting its potential for clinical use.

Conclusions

In this study, hydrogels were prepared by using GelMA and AHA through Schiff base and covalent bonding, and the residual aldehyde group of AHA was used to interact with the amino group of Gel@Cur nanoparticles, which successfully overcame the disadvantage of Gel@Cur nanoparticles' susceptibility to agglomeration and at the same time endowed the composite hydrogels with more excellent properties. Due to the nano-toughening effect, the introduction of Gel@Cur nanoparticles led to an increase in the mechanical strength of the hydrogel. In addition, the encapsulation of the nanoparticles with the hydrogel backbone allowed the slow release of curcumin, resulting in the formation of a GelMA/AHA-Gel@Cur composite hydrogel with significant antimicrobial and pro-infective wound repair capabilities. Through in vitro drug release simulation experiments, we found that the drug release mechanism of the hydrogel was a combination of drug diffusion and backbone dissolution. The composite hydrogel also had good cytocompatibility and haemocompatibility, and HUVECs cells cultured with its extracts proliferated rapidly and had good morphology. The haemocompatibility test showed that the haemolysis rate of the hydrogel was 0.45%. In conclusion, GelMA/AHA-Gel @Cur composite hydrogel has good mechanical properties, antimicrobial properties and drug slow-release ability, as well as excellent cytocompatibility and haemocompatibility, which can promote the repair of infected wounds, and it is a very promising wound repair material, which is expected to be applied to the clinical treatment of skin infected wounds.

Acknowledgments

The authors are grateful to the Natural Science Foundation of Guangdong Province (No.2021A1515111158) and the National Natural Science Foundation of China (No.32300962) for supporting this study. The authors would like to thank the Guangxi Kanghua Regenerative Medicine Biotechnology Co., LTD for providing the facilities and resources necessary for this research.

Disclosure

The authors declare that they have no potential conflicts of interest regarding the research, authorship, and/or publication of this article.

References

1. Lim HW, Kohli I, Ruvolo E, Kolbe L, Hamzavi IH. Impact of visible light on skin health: the role of antioxidants and free radical quenchers in skin protection. *J Am Acad Dermatol*. 2022;86(3):S27–S37. doi:10.1016/j.jaad.2021.12.024
2. Kortekaas Krohn I, Aerts JL, Breckpot K, et al. T-cell subsets in the skin and their role in inflammatory skin disorders. *Allergy*. 2021;77(3):827–842. doi:10.1111/all.15104
3. Michalak M. Plant-Derived Antioxidants: significance in Skin Health and the Ageing Process. *Int J Mol Sci*. 2022;23(2):585. doi:10.3390/ijms23020585
4. Dokoshi T, Chen Y, Cavagnero KJ, et al. Dermal injury drives a skin to gut axis that disrupts the intestinal microbiome and intestinal immune homeostasis in mice. *Nat Commun*. 2024;15(1):3009. doi:10.1038/s41467-024-47072-3
5. Kang K, Ye S, Jeong C, et al. Bionic artificial skin with a fully implantable wireless tactile sensory system for wound healing and restoring skin tactile function. *Nat Commun*. 2024;15(1):10. doi:10.1038/s41467-023-44064-7
6. Li Q, Jia C, Pan W, et al. Multi-omics study reveals different pathogenesis of the generation of skin lesions in SLE and IDLE patients. *J Autoimmun*. 2024;146:103203. doi:10.1016/j.jaut.2024.103203
7. Hong Z-X, Zhu S-T, Li H, et al. Bioengineered skin organoids: from development to applications. *Military Med Res*. 2023;10(1):40. doi:10.1186/s40779-023-00475-7
8. Liu S, He S, Chen C, et al. A Versatile Disorder-to-Order Technology to Upgrade Polymers into High-Performance Bioinspired Materials. *Adv Healthcare Mater*. 2023;12(22):2300068. doi:10.1002/adhm.202300068
9. Lou P, Liu S, Wang Y, et al. Neonatal-Tissue-Derived Extracellular Vesicle Therapy (NEXT): a Potent Strategy for Precision Regenerative Medicine. *Adv Mater*. 2023;35(33):2300602. doi:10.1002/adma.202300602
10. Chen Y, Lu W, Zhou Y, et al. A Spatiotemporal Controllable Biomimetic Skin for Accelerating Wound Repair. *Small*. 2024;20:2310556. doi:10.1002/smll.202310556
11. Ji S, Li Y, Xiang L, et al. Cocktail Cell-Reprogrammed Hydrogel Microspheres Achieving Scarless Hair Follicle Regeneration. *Adv Sci*. 2024;11:2306305. doi:10.1002/advs.202306305

12. Ross A, Guo X, Salazar GAM, et al. Multipurpose On-the-Spot Peptide-Based Hydrogels for Skin, Cornea, and Heart Repair. *Adv Funct Mater*. 2024;34:2402564. doi:10.1002/adfm.202402564
13. Lu Y, Zhao M, Peng Y, et al. A physicochemical double-cross-linked gelatin hydrogel with enhanced antibacterial and anti-inflammatory capabilities for improving wound healing. *J Nanobiotechnol*. 2022;20(1):426. doi:10.1186/s12951-022-01634-z
14. Xu L, Zhang Z, Jorgensen AM, et al. Bioprinting a skin patch with dual-crosslinked gelatin (GelMA) and silk fibroin (SilMA): an approach to accelerating cutaneous wound healing. *Mater Today Bio*. 2023;18:100550. doi:10.1016/j.mtbio.2023.100550
15. Liu C, Dai T, Wu X, et al. 3D bioprinting of cell-laden nano-attapulgite/gelatin methacrylate composite hydrogel scaffolds for bone tissue repair. *J Mater Sci Technol*. 2023;135:111–125. doi:10.1016/j.jmst.2022.07.011
16. Wang J-H, Tsai C-W, Tsai N-Y, et al. An injectable, dual crosslinkable hybrid pectin methacrylate (PECMA)/gelatin methacryloyl (GelMA) hydrogel for skin hemostasis applications. *Int J Biol Macromol*. 2021;185:441–450. doi:10.1016/j.ijbiomac.2021.06.162
17. Wu J, Xiao Z, Chen A, et al. Sulfated zwitterionic poly (sulfobetaine methacrylate) hydrogels promote complete skin regeneration. *Acta Biomater*. 2018;71:293–305. doi:10.1016/j.actbio.2018.02.034
18. Salehi B, Rodrigues CF, Peron G, et al. Curcumin nanoformulations for antimicrobial and wound healing purposes. *Phytother Res*. 2021;35 (5):2487–2499. doi:10.1002/ptr.6976
19. Alqahtani MS, Alqahtani A, Kazi M, et al. Wound-healing potential of curcumin loaded lignin nanoparticles. *J Drug Delivery Sci Technol*. 2020;60:102020. doi:10.1016/j.jddst.2020.102020
20. Wu S, Zhu L, Ni S, et al. Hyaluronic acid-decorated curcumin-based coordination nanomedicine for enhancing the infected diabetic wound healing. *Int J Biol Macromol*. 2024;263:130249. doi:10.1016/j.ijbiomac.2024.130249
21. Long S, Yu M-J, Feng R, Tao H, Zhang B. Novel self-assembled micelles of dual-modified dextrin with pH responsiveness via grafted octenyl succinic anhydride and cysteamine for curcumin delivery. *Food Chem*. 2024;460:140748. doi:10.1016/j.foodchem.2024.140748
22. Gottschalk J, Aßmann M, Kuballa J, Elling L. Repetitive Synthesis of High-Molecular-Weight Hyaluronic Acid with Immobilized Enzyme Cascades. *ChemSusChem*. 2022;15(9):e202101071. doi:10.1002/cssc.202101071
23. Buffa R, Nešporová K, Basarabová I, Halamková P, Svozil V, Velebný V. Synthesis and study of branched hyaluronic acid with potential anticancer activity. *Carbohydr. Polym.* 2019;223:115047. doi:10.1016/j.carbpol.2019.115047
24. Li J, Qiao M, Ji Y, Lin L, Zhang X, Linhardt RJ. Chemical, enzymatic and biological synthesis of hyaluronic acids. *Int J Biol Macromol*. 2020;152:199–206. doi:10.1016/j.ijbiomac.2020.02.214
25. Li J, Zhao M, Liang J, et al. Hollow CuS immobilized in polysaccharide hydrogel promotes photothermally-driven vascularization. *Chem Eng J*. 2024;481:148287. doi:10.1016/j.cej.2023.148287
26. Li Y, Miao Y, Yang L, et al. Recent advances in the development and antimicrobial applications of metal–phenolic networks. *Adv Sci*. 2022;9 (27):2202684. doi:10.1002/advs.202202684
27. Niu W, Chen M, Guo Y, et al. A multifunctional bioactive glass-ceramic nanodrug for post-surgical infection/cancer therapy-tissue regeneration. *ACS nano*. 2021;15(9):14323–14337. doi:10.1021/acsnano.1c03214
28. Tan H, Zhang R, Han L, Zhang T, Ngai T. Pickering emulsions stabilized by aminated gelatin nanoparticles: are gelatin nanoparticles acting as genuine Pickering stabilizers or structuring agents? *Food Hydrocoll*. 2022;123:107151. doi:10.1016/j.foodhyd.2021.107151
29. Madkhali O, Mekhail G, Wettig SD. Modified gelatin nanoparticles for gene delivery. *Int J Pharm*. 2019;554:224–234. doi:10.1016/j.ijpharm.2018.11.001
30. Yasmin R, Shah M, Khan SA, Ali R. Gelatin nanoparticles: a potential candidate for medical applications. *Nanotechnol Rev*. 2017;6(2):191–207. doi:10.1515/ntrev-2016-0009
31. Gao Y, Meng S, Liu W, et al. Physical contact-triggered in situ reactivation of antibacterial hydrogels. *ACS Appl. Mater Inter*. 2023;15 (6):7735–7746. doi:10.1021/acsami.2c19113
32. Jiang Y, Wang L, Qi W, et al. Antibacterial and self-healing sepiolite-based hybrid hydrogel for hemostasis and wound healing. *Biomat Adv*. 2024;159:213838. doi:10.1016/j.bioadv.2024.213838
33. Zhao P, Feng Y, Zhou Y, Tan C, Liu M. Gold@ Halloysite nanotubes-chitin composite hydrogel with antibacterial and hemostatic activity for wound healing. *Bioact Mater*. 2023;20:355–367. doi:10.1016/j.bioactmat.2022.05.035
34. Shen C, Zhao X, Ren Z, et al. In Situ Formation of Injectable Gelatin Methacryloyl (GelMA) Hydrogels for Effective Intraocular Delivery of Triamcinolone Acetonide. *Int J Mol Sci*. 2023;24(5):4957. doi:10.3390/ijms24054957
35. Wang J, Wang X, Liang Z, et al. Injectable antibacterial Ag-HA/GelMA hydrogel for bone tissue engineering. *Front Bioeng Biotechnol*. 2023;11:1219460. doi:10.3389/fbioe.2023.1219460
36. Wang Z, Tian Z, Menard F, Kim K. Comparative study of gelatin methacrylate hydrogels from different sources for biofabrication applications. *Biofabrication*. 2017;9(4):044101. doi:10.1088/1758-5090/aa83cf
37. Hu J, Chen Y, Li Y, Zhou Z, Cheng Y. A thermo-degradable hydrogel with light-tunable degradation and drug release. *Biomaterials*. 2017;112:133–140. doi:10.1016/j.biomaterials.2016.10.015
38. Lou C, Tian X, Deng H, Wang Y, Jiang X. Dialdehyde-β-cyclodextrin-crosslinked carboxymethyl chitosan hydrogel for drug release. *Carbohydr Polym*. 2020;231:115678. doi:10.1016/j.carbpol.2019.115678
39. Edirisinghe DIU, D'Souza A, Ramezani M, et al. Antibacterial and Cytocompatible pH-Responsive Peptide Hydrogel. *Molecules*. 2023;28 (11):4390. doi:10.3390/molecules28114390
40. Lopes SV, Walczak P, Janowski M, Reis RL, Silva-Correia J, Oliveira JM. Cytocompatible manganese dioxide-based hydrogel nanoreactors for MRI imaging. *Biomat Adv*. 2022;134:112575. doi:10.1016/j.msec.2021.112575
41. Trujillo S, Kasper J, de Miguel-Jiménez A, et al. Cytocompatibility evaluation of PEG-methylsulfone hydrogels. *ACS omega*. 2023;8 (35):32043–32052. doi:10.1021/acsomega.3c03952
42. Zhang M, Chan CH, Pauls JP, et al. Investigation of heparin-loaded poly (ethylene glycol)-based hydrogels as anti-thrombogenic surface coatings for extracorporeal membrane oxygenation. *J Mat Chem B*. 2022;10(26):4974–4983. doi:10.1039/D2TB00379A
43. Shi L, Zeng Y, Zhao Y, et al. Biocompatible injectable magnetic hydrogel formed by dynamic coordination network. *ACS Appl Mater Interf*. 2019;11(49):46233–46240. doi:10.1021/acsami.9b17627
44. Tang L, Xu C, Xuan A, Zhu Z, Ruan D. Functionalized self-assembling peptide RADKPS hydrogels promote regenerative repair of degenerated intervertebral discs. *Biomater. Sci.* 2022;10(18):5134–5145. doi:10.1039/D2BM00634K

45. Wintjens AG, Fransen PPK, Lenaerts K, et al. Development of a supramolecular hydrogel for intraperitoneal injections. *Macromol biosci*. 2024;24 (1):2300005. doi:10.1002/mabi.202300005
46. Du M, Jin J, Zhou F, Chen J, Jiang W. Dual drug-loaded hydrogels with pH-responsive and antibacterial activity for skin wound dressing. *Colloids Surf B*. 2023;222:113063. doi:10.1016/j.colsurfb.2022.113063
47. Chen S, Wang Y, Lai J, Tan S, Wang M. Structure and properties of gelatin methacryloyl (GelMA) synthesized in different reaction systems. *Biomacromolecules*. 2023;24(6):2928–2941. doi:10.1021/acs.biomac.3c00302
48. Wang Z, Liu J, Zheng Y, et al. Copper Ion-Inspired Dual Controllable Drug Release Hydrogels for Wound Management: driven by Hydrogen Bonds. *Small*. 2024;20:2401152. doi:10.1002/smll.202401152
49. Zhai X, Wu Y, Tan H. Gelatin-based targeted delivery systems for tissue engineering. *Current Drug Targ*. 2023;24(8):673–687. doi:10.2174/ 1389450124666230605150303